Polymer passivation of defects in inorganic perovskite solar cells*

ZHANG Meng[1], ZHANG Fanghui[2], SHI Kewang[2], ZHANG Wenxi[1], HUANG Jin[2], and QIU Huimin[1]**

1. School of Electrical and Control Engineering, Shaanxi University of Science & Technology, Xi'an 710021, China

2. School of Electronic Information and Artificial Intelligence, Shaanxi University of Science and Technology, Xi'an 710021, China

(Received 8 December 2021; Revised 21 January 2022)

Inorganic perovskite solar cells (IPSCs) have attained attention due to their excellent thermal and phase stability. In this work, we demonstrate a novel approach for fabricating IPSCs, using the strategies of interface passivation and anti-solvent before spin-coating perovskite. Poly(methyl methacrylate) (PMMA) and chlorobenzene (CB) are used as passivator and anti-solvent, respectively. The CB improves the perovskite crystal morphology. Meanwhile, PMMA passivates the defects between poly(3, 4-ethylenedioxythiophene)-poly(styrenesulfonate) (PEDOT: PSS) and perovskite layer, thus increasing the short-circuit current. Excitingly, we find that PMMA benefits the grain boundaries (GBs) of perovskite, which makes it more humidity-resistant, increasing the stability of perovskite film. Especially, PMMA mitigates interfacial charge losses, and the devices based on $CsPbI_{3-x}Br_x$ passivated by PMMA exhibit the power conversion efficiency (*PCE*) much higher than those based on pure $CsPbI_{3-x}Br_x$.

Document code: A **Article ID:** 1673-1905(2022)06-0338-5

DOI https://doi.org/10.1007/s11801-022-1187-6

In the past decade, the power conversion efficiency (*PCE*) of the perovskite solar cells (PSCs) had already surpassed that of monocrystalline silicon solar cells, and the efficiency reached a staggering 25%[1,2]. Perovskite materials have the advantages of adjustable bandgap, high absorption coefficient, long carrier lifetime, and high carrier mobility[3-5]. However, the organic-inorganic hybrid perovskite tends to degrade under heat or humid conditions, which originates from their organic cations. As a direct bandgap semiconductor, its conduction band and valence band energy levels are hybridized by the sp orbitals of boron (B) and X elements, and the bandgap is adjustable[2]. The stability of the cubic structure is determined by the Schmidt tolerance factor[6]. The inorganic perovskite $CsPbX_3$ (X=Cl, Br, I) owes a suitable energy bandgap, which is great to configure a tandem device. $CsPbI_3$ owes a suitable energy bandgap of 1.7 eV[7-9]. However, black $CsPbI_3$ with poor stability easily converts to its yellow δ-phase in the ambient atmosphere. Therefore, the stabilization of the α-$CsPbI_3$ phase is an important factor in the fabrication of all-inorganic perovskite solar cells (IPSCs). An obvious way of tuning the tolerance factor of the cubic phase is partially substituting iodide with the smaller radius, further stabilizing the α-phase by incorporating Br^- ions into the lattice[10,11].

Inverted PSCs (p-i-n structure) have been becoming more and more attractive, owing to their easy fabrication, cost-effectiveness, and suppressed hysteresis characteristics[12,13]. In such a structure, common hole transport material (HTM) is poly(3, 4-ethylenedioxythiophene)-poly-(styrenesulfonate) (PEDOT: PSS) and electron transport material (ETM) is [6,6]-phenyl-C_{61}-butyric acid methyl ester (PCBM)[14-16]. We made the inverted PSCs with a structure of FTO/PEDOT: PSS/$CsPbI_{3-x}Br_x$/PCBM/Al, which is a simple structure in an inverted structure[17]. High-quality perovskite film is the key to high-efficiency solar cells[18]. Although the PEDOT: PSS thin film exhibited excellent performance, there are lots of defects in PEDOT: PSS and perovskite interface. And solution prepared $CsPbI_{3-x}Br_x$ films usually have lots of defects that demand to be passivated and also their degradations often happen at the grain boundaries (GBs) of the perovskite[19]. Poly(methyl methacrylate) (PMMA) can be passivation effect of perovskite films by reducing the surface traps or filling the cracks[19-21]. In our process of fabricating solar cell devices, the temperature is not higher than 210 ℃.

Anhydrous ethanol and chlorobenzene (CB) were purchased from Sinopharm Chemical Reagent Co., Ltd. The PMMA was purchased from Sigma-Aldrich. Lead

* This work has been supported by the National Natural Science Foundation of China (Nos.61904100 and 11604194), and the Education Department of Shaanxi Province Serves the Local Special Plan Project (No.17JF006).

** E-mail: zhangfanghui@sust.edu.cn

bromide ($PbBr_2$, 99.99%), lead iodide (PbI_2, 99.99%), cesium iodide (CsI, 99.99%), and PEDOT: PSS (Clevios PVP, AI 4083) solution were purchased from Xi'an Polymer Light Technology Corporation. Hydroiodic acid (HI, 57 wt.% in water), N, N Dimethylformamide (DMF 99.8%) and Dimethyl sulfoxide (DMSO 99.9+%) were purchased from Alfa Aesar. The PCBM (99%) came from Solenne B.V. The F-doped SnO_2 (FTO) glasses were purchased from Yingkou Libra New Energy Technology Co., Ltd.

$DMAPbI_3$ ($DMA=(CH_3)_2NH_2^+$) precursor was prepared by dissolving PbI_2 (2.3 g) in DMF (5 mL), and when PbI_2 was dissolved completely, HI was added, stirred at 70 °C for 6 h to ensure complete reaction. The precursor was washed in diethyl ether to obtain the light-yellow precipitate. Next, the yellow powder was obtained and dried overnight in a 50 °C vacuum oven[22,23].

To prepare the inorganic perovskite precursor solution, CsI (0.187 0 g), $DMAPbI_3$ (0.380 4 g) and $PbBr_2$ (0.073 4 g) were dissolved in solvent of 1 mL DMF/DMSO (volume ratio of 850: 150). The solution was stirred at room temperature for 3 h for complete dissolution and was used after filtering. Dilute the PEDOT: PSS with water (volume ratio of 1: 2), used after filtering. To prepare PMMA solution, the PMMA (5 mg) was dissolved in CB (5 mL). For PCBM solution, the PCBM (40 mg) was dissolved in CB (2 mL). A small amount of PMMA was added to the antisolvent CB and dripped on the hole transport layer before the perovskite film was spin-coated, and the perovskite layer was spun directly without annealing.

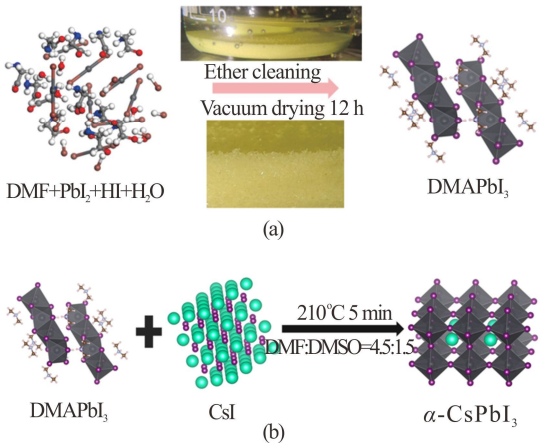

Fig.1 (a) $DMAPbI_3$ synthetic diagram; (b) Perovskite synthetic diagram

Firstly, FTO glasses (2.5 cm×2.5 cm) were washed with deionized water, acetone and ethanol in ultrasonic cleaner. Then FTO glasses were treated in O_2 plasma cleaner for 3 min. For an HTM, the PEDOT: PSS solution was spin-coated on the FTO substrates with 6 000 rpm for 30 s. Afterward, the substrates were heated on a hot plate in air at 210 °C for 10 min. The control group spin-coated the perovskite layer at 4 000 rpm for 30 s directly. Other group spin-coated 100 μL PMMA solutions with different concentrations (0 mg/mL, 0.5 mg/mL, 1 mg/mL, 1.5 mg/mL) were coated on the PEDOT: PSS film at 4 000 rpm for 30 s then spin-coated the perovskite films immediately, finally annealed at 200 °C for 5 min. For an ETM, the PCBM solution was coated on the perovskite films at 4 000 rpm for 30 s and then annealed at 100 °C for 10 min. Finally, 100-nm-thick Al electrode was prepared on ETM film by thermal evaporation method to accomplish the device fabrication.

Current-voltage (*J-V*) characteristics were measured in dry air by a Keithley 2400 source meter under standard 1 sun AM 1.5 simulated solar irradiation system (SAN-EI 100 $mW \cdot cm^{-2}$) from Giant Force Technology Co., Limited. Ultraviolet-visible (UV-Vis) spectra were collected on the UV-2600 UV-Vis spectrophotometer (Sunny optical technology (group) Co., Ltd., Ningbo, China). Steady photoluminescence (PL) spectra were recorded on a fluorescence spectrophotometer (Hitachi F-7000) with a 535 nm excitation. X-ray diffraction (XRD) patterns of the perovskite film samples were measured by Bruker D8 DISCOVER with Cu Kα radiation (1.540 5 Å). The PL spectra were obtained by a spectrophotometer (Flurolog, Horiba Jobon Yvon), and the excitation wavelength was 510 nm. Scanning electron microscope (SEM) used TESCAN VEGA3 SBH.

Fig.2 shows the spin coating and annealing processes of the perovskite film. We see that the color changed during the spin coating process of the perovskite solution. Annealing on a heating table at 200 ℃ for 5 min can form a black film. In fact, it looks like a dark brown semitransparent film because some visible light can pass through it.

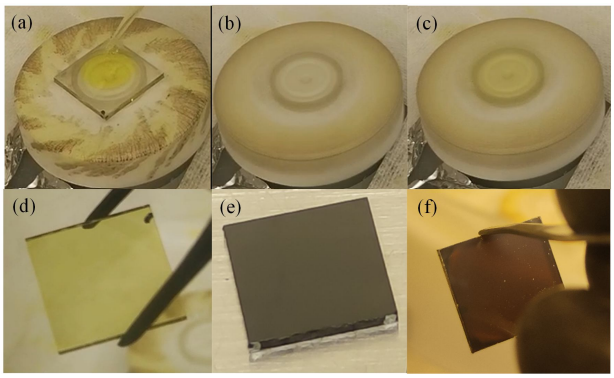

Fig.2 (a)—(c) Spin coating and (d)—(f) annealing processes of perovskite film

Fig.3(a) compares the UV-Vis diffusion absorption of different phases of perovskite. The α-$CsPbI_{3-x}Br_x$ shows excellent visible light absorption performance, and the black phase of the perovskite phase changes to the δ-$CsPbI_{3-x}Br_x$ yellow phase due to water and oxygen erosion, so light absorption is significantly reduced.

Therefore, the stable existence of black phase perovskite is a necessary condition for making high efficiency PSCs. A Tauc plot is used to determine the optical bandgap of semiconductors. As shown in Fig.3(b) and (c), Tauc plots of the α-$CsPbI_{3-x}Br_x$ and δ-$CsPbI_{3-x}Br_x$ show that the black phase bandgap is 1.74 eV and yellow phase bandgap is 2.88 eV. The phase had been changed, and the bandgap of perovskite became bigger. It means higher energy photons are absorbed, which is not conducive to the absorption of visible light, making PSCs devices efficiency reduced.

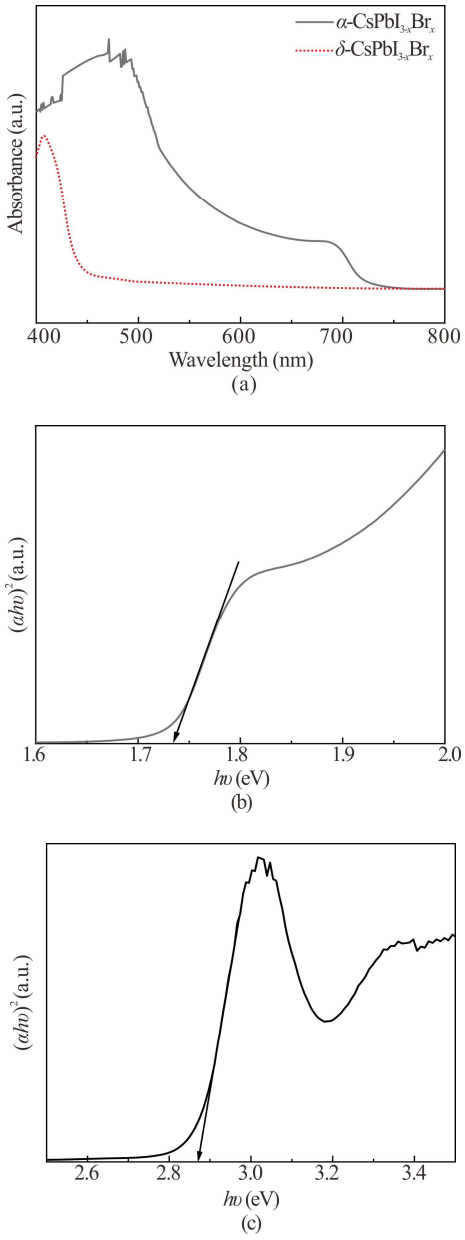

Fig.3 (a) UV-Vis absorbance spectra of α-$CsPbI_{3-x}Br_x$ and δ-$CsPbI_{3-x}Br_x$; Tauc plot curves of (b) α-$CsPbI_{3-x}Br_x$ and (c) δ-$CsPbI_{3-x}Br_x$

Fig.4 displays the structure of the solar cells and the energy band alignments. The photon was absorbed by the perovskite layer, an electron hole pair was generated, and electron transition from the valence band to the conduction band appeared. Then, the electrons and holes flowed from the conduction band of PCBM and the valence band of PEDOT: PSS to the electrode. Conduction band and valence band of absorption layer and other layers matching is also an important factor affecting efficiency. We note that PMMA can effectively prevent electrons from moving to the HTM layer. However, holes can move towards HTM layer due to quantum tunneling.

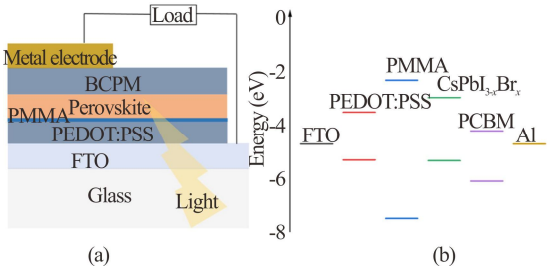

Fig.4 (a) Schematic structure of the PSCs and (b) energy band alignments

Fig.5 compares the XRD patterns of perovskite absorbers films with those of the CB solutions with different concentrations of PMMA. All the samples presenting strong perovskite characteristic peaks are identified as (100) and (200) located at 14.3° and 28.9° with the same intensities, indicating that the PMMA treatment neither induces the formation of new phases nor affects the crystallinity of the obtained perovskite films. Therefore, this passivation treatment has a negligible effect on crystallinity.

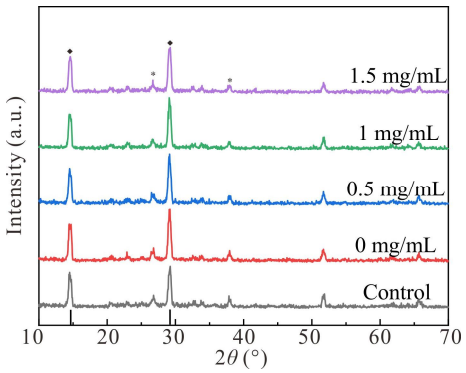

Fig.5 XRD pattern of perovskite thin films with different concentrations of PMMA

Steady-state PL results of the perovskite films with different concentrations of PMMA and without PMMA are shown in Fig.6. The perovskite films all exhibit a band edge of ~714 nm. Apparently, the optimized film exhibits a higher PL intensity than the control film. The results indicate that the defects of optimized film are significantly reduced.

$$E = 1\,240/\lambda\,. \tag{1}$$

Through Eq.(1) of the relationship between wavelength and energy, we can calculate the corresponding photon energy is 1.74 eV, corresponding to a bandgap of inorganic perovskite $CsPbI_{3-x}Br_x$.

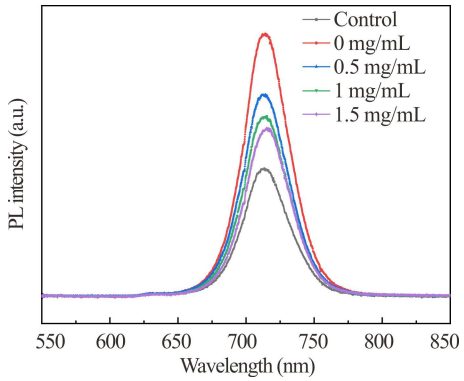

Fig.6 PL spectra for perovskite films with different concentrations of PMMA

To intuitively acquire the result of PMMA acting on the morphology of $CsPbI_{3-x}Br_x$ perovskite film, the top-view SEM images are shown in Fig.7. It is observed from Fig.7(a) that lots of pores are distributed on the surface of the control group. When the CB solutions with different concentrations of PMMA increased from 0 mg/mL to 1.5 mg/mL were added, the number of pores decreased and the surface of the films became denser. But the perovskite film became uneven when PMMA concentration was 1.5 mg/mL.

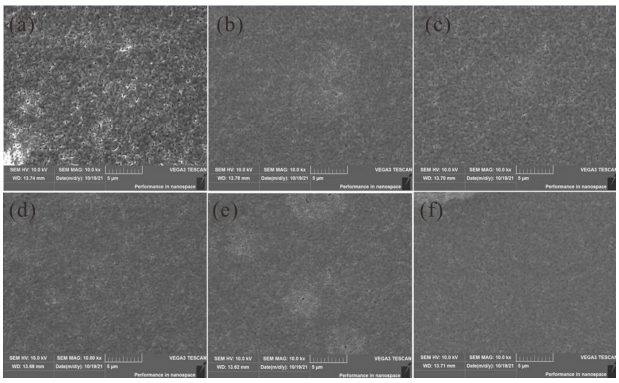

Fig.7 Top-view SEM images of perovskite films with different concentrations of PMMA: (a) Control group; (b) 0 mg/mL; (c) 0.5 mg/mL; (d) 1 mg/mL; (e) 1.5 mg/mL; (f) Top-view SEM image of PCBM films

In order to evaluate the humidity stability, the stability of perovskite films was tested in air, as shown in Fig.8. The color trends were observed when perovskites degraded in a humid environment. The PMMA-treated perovskite film exhibited higher stability than pure perovskite film. The improved stability of the perovskite films could be attributed to that PMMA can passivate the GB of perovskite films.

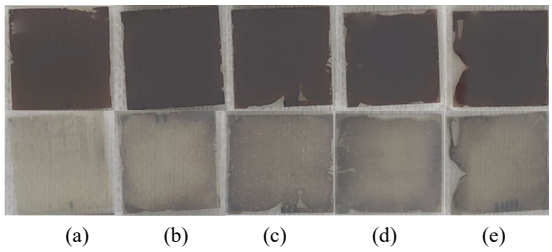

Fig.8 Photographs of perovskite films with different concentrations of PMMA at different time

Fig.9 shows *J-V* curves of the solar cells. The common performance parameters, such as V_{oc}, short circuit current density (J_{sc}), fill factor (*FF*), and *PCE*, are listed in Tab.1.

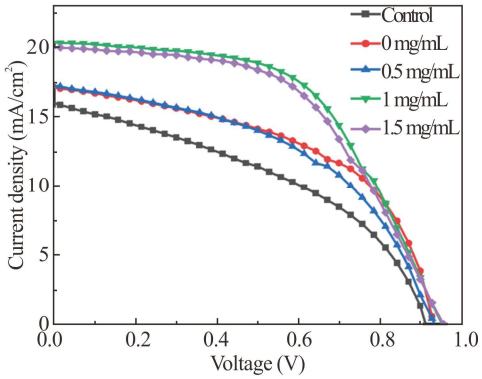

Fig.9 *J-V* curves of the solar cells with different concentrations of PMMA

Tab.1 PSCs with different PMMA passivated contents under an AM 1.5 illumination (100 mW/cm^2)

Sample	J_{sc} (mA·cm^{-2})	V_{oc} (V)	*FF* (%)	*PCE* (%)
Control	15.98	0.92	41.16	6.06
0 mg/mL	17.24	0.93	47.57	7.67
0.5 mg/mL	17.12	0.93	51.33	8.20
1 mg/mL	20.36	0.95	54.80	10.63
1.5 mg/mL	20.03	0.95	52.93	10.14

We can see the *PCE* of the solar cells is increased from 6.06% to 10.14%, because the J_{sc} is increased, and the *FF* is also increased. We consider the possible reason of the improved device performance upon the addition of the PMMA interlayer. We think PMMA could form a thin layer where tunnelling effect is strongly. It can effectively prevent the recombination of electrons in HTM layer, and PMMA could effectively passivate the perovskite at surface and its GBs.

In summary, we fabricated inverted structure IPSCs and we demonstrated that the insertion of an insulating PMMA layer could improve J_{sc} and *FF*. We find that our PMMA-based devices exhibited 40% improvement in *PCE* relative to the control solar cells. Thus, the PMMA passivation treatment presents to improve IPSCs and

opens a window to design outstanding perovskite optoelectronics for future applications.

Statements and Declarations

The authors declare that there are no conflicts of interest related to this article.

References

[1] TIAN J J, XUE Q F, YAO Q, et al. Inorganic halide perovskite solar cells：progress and challenges[J]. Advanced energy materials, 2020, 10(23)：2000183.

[2] LI Z Z, ZHOU F G, WANG Q, et al. Approaches for thermodynamically stabilized $CsPbI_3$ solar cells[J]. Nano energy, 2020, 71：104634.

[3] PARIDA B, RYU J, YOON S, et al. Two-step growth of $CsPbI_{3-x}Br_x$ films employing dynamic CsBr treatment：toward all-inorganic perovskite photovoltaics with enhanced stability[J]. Journal of materials chemistry, 2019, 7(31)：18488-18498.

[4] FU Q, TANG X, HUANG B, et al. Recent progress on the long-term stability of perovskite solar cells[J]. Advanced science, 5(5)：1700387.

[5] BACK H, KIM G, KIM J, et al. Achieving long-term stable perovskite solar cells via ion neutralization[J]. Energy & environmental science, 2016, 9(4)：1258-1263.

[6] GREEN M A, HO-BAILLIE A, SNAITH H J. The emergence of perovskite solar cells[J]. Nature photonics, 2014, 8(7)：506-514.

[7] WANG Y, ZHANG T, KAN M, et al. Efficient α-$CsPbI_3$ photovoltaics with surface terminated organic cations[J]. Joule, 2018, 2(10)：2065-2075.

[8] WANG K, JIN Z, LIANG L, et al. Chlorine doping for black γ-$CsPbI_3$ solar cells with stabilized efficiency beyond 16%[J]. Nano energy, 2019, 58：175-182.

[9] KE F, WANG C, JIA C, et al. Preserving a robust $CsPbI_3$ perovskite phase via pressure-directed octahedral tilt[J]. Nature communications, 2021, 12(1)：1-8.

[10] LIU C, LI W, ZHANG C, et al. All-inorganic $CsPbI_2Br$ perovskite solar cells with high efficiency exceeding 13%[J]. Journal of the American Chemical Society, 2018,140(11)：3825-3828.

[11] SHANG Y, FANG Z, HU W, et al. Efficient and photostable $CsPbI_2Br$ solar cells realized by adding PMMA[J]. Journal of semiconductors, 2021, 42(5)：050501.

[12] LIU T H, CHEN K, HU Q, et al. Inverted perovskite solar cells：progresses and perspectives[J]. Advanced energy materials, 2016, 6(17)：1600457.

[13] CHEN K, HU Q, LIU T, et al. Charge-carrier balance for highly efficient inverted planar heterojunction perovskite solar cells[J]. Advanced materials, 2016, 28(48)：10718-10724.

[14] XIA Y, DAI S. Review on applications of PEDOTs and PEDOT：PSS in perovskite solar cells[J]. Journal of materials science：materials in electronics, 2020, 32(10)：12746-12757.

[15] RAHAQ Y, MOUSSA M, MOHAMMAD A, et al. Highly reproducible perovskite solar cells via controlling the morphologies of the perovskite thin films by the solution-processed two-step method[J]. Journal of materials science-materials in electronics, 2018, 29(19)：16426-16436.

[16] CHEN C L, ZHANG S S, WU S H, et al. Effect of BCP buffer layer on eliminating charge accumulation for high performance of inverted perovskite solar cells[J]. Royal society of chemistry advances, 2017, 7(57)：35819-35826.

[17] TSAI C H, LIN C M, KUEI C H. Investigation of the effects of various organic solvents on the PCBM electron transport layer of perovskite solar cells[J]. Coatings, 2020, 10(3)：273.

[18] ZHANG T, WANG F, CHEN H, et al. Mediator antisolvent strategy to stabilize all-inorganic $CsPbI_3$ for perovskite solar cells with efficiency exceeding 16%[J]. ACS energy letters, 2020, 5(5)：1619-1627.

[19] YUAN B L, LI C, YI W C, et al. PMMA passivated $CsPbI_2Br$ perovskite film for highly efficient and stable solar cells[J]. Journal of physics and chemistry of solids, 2021, 153：110000.

[20] AVA T T, JEONG H J, YU H M, et al. Role of PMMA to make $MAPbI_3$ grain boundary heat-resistant[J]. Applied surface science, 2021, 558：149852.

[21] DING D, LANZETTA L, LIANG X, et al. Ultrathin polymethylmethacrylate interlayers boost performance of hybrid tin halide perovskite solar cells[J]. Chemical communications, 2021, 57(41)：5047-5050.

[22] WANG F, YU H, XU H H, et al. $HPbI_3$：a new precursor compound for highly efficient solution-processed perovskite solar cells[J]. Advanced functional materials, 2015, 25(7)：1120-1126.

[23] PEI Y, LIU Y, LI F, et al. Unveiling property of hydrolysis-derived $DMAPbI_3$ for perovskite devices：composition engineering, defect mitigation, and stability optimization[J]. IScience, 2019, 15：165-172.